Suspensions with small, spherical particles

SA104X Degree Project in Engineering Physics

Samuel Zackrisson[1]
Supervisor: Anna-Karin Tornberg[2]

[2]Numerical Analysis, Royal Institute of Technology (KTH)
[1]samuelz@kth.se
[2]akto@kth.se

May 20, 2015

Feasibly computable analytic solutions for systems of many particles in fluid dynamics and electrostatics are few and far-between. Simulations and numerical approximations are essential to studying these systems. This is commonly done without directly calculating the interacting field between particles. Simply storing a discretized field in a three dimensional setting on a cubic $N \times N \times N$-grid is $O(N^3)$, so finding efficient and accurate methods are of great interest. In this report a method utilizing the spectral accuracy of the Fourier transform is studied. The method is applied to a ball of particles sedimenting in a fluid affected by gravity. The properties of this method are compared to similar studies of the same system. The purpose is to map and evaluate the properties of this method in comparison with present work.

Contents

1 Introduction

1.1 Sedimenting suspensions of small particles

Feasibly computable analytic solutions for systems of many particles in fluid dynamics and electrostatics are few and far-between. Simulations and numerical approximations are essential to studying these systems. This is commonly done without directly calculating the interacting field between particles. Simply storing a discretized field in a three dimensional setting on a cubic $N \times N \times N$-grid is $O(N^3)$, so finding efficient and accurate methods are of great interest. Finding fast methods of performing calculations on this large set can be simplified by making the assumption of a periodic grid - assuming that the N^3-point cube is replicated much like the primitive cells of a crystal lattice. This introduces a periodicity which makes room for Fourier methods and - for smooth functions - spectral (exponential) convergence in solutions and the use of the fast Fourier transform, which in some places reduced the complexity to $O(NlogN)$ [5]. In this project a specific method of using the Fourier transform is studied, applied to a ball of particles sedimenting in a fluid affected by gravity, and compared to similuar studies of the same system. The purpose is to evaluate this method in comparison with present work on the same simulation.

1.2 Purpose of this study

To implement a spectral method for simulation of small, spherical particles sedimenting in a fluid.
To verify some fundamental properties of the methods used.
To compare this method to other methods employed by others. This is done by looking at convergence, differences in flow etc.
To compare how this method introduces new and preserves macroscopic phenomena, compared to how the other methods behave.

2 Theory

2.1 Stokes flow

For the small particles in an incompressible, viscous fluid in this study, the Reynolds number is assumed to be small ($Re << 1$). The general Navier-Stokes equations can under these conditions be approximated as a linear set of equations, the steady Stokes equations. A solution to these equations is called as a *Stokes flow*. For more details on the equations as they appear here, see [2].
The continuity equation for an incompressible fluid appears as

$$\nabla \cdot \mathbf{u} = 0, \tag{1}$$

and the equations for conservation of momentum are

$$\mu\nabla^2\mathbf{u} = \nabla p - \mathbf{f}. \tag{2}$$

Here μ is the dynamic viscosity of the fluid, $\mathbf{u} = (u_1, u_2, u_3)$ is the velocity field of the fluid, p is the absolute pressure and $\mathbf{f} = (f_1, f_2, f_3)$ is the volume force on the fluid, the *forcing function*. $\mathbf{u}$, p and $\mathbf{f}$ are multivariate functions on $\mathbf{R}^3$.

The particle system is assumed to be periodic in three dimensions, i.e. the system and all its characteristics within the volume $[0, L)^3$ is assumed to repeat in the x-,y- and z-directions. In terms of $\mathbf{f}$,

$$\mathbf{f}(\mathbf{r}) = \mathbf{f}(\mathbf{r} + L\mathbf{m}),\ \forall\mathbf{m} \in \mathbb{Z}^3. \tag{3}$$

Thus if $\mathbf{f}$ is known in $[0, L)^3$, it is known in $\mathbf{R}^3$. Analogously $\mathbf{u}$ and p are assumed to be periodic.

2.2 Fourier analysis

Studying the Stokes equations (1) and (2) in Fourier space one can find an explicit solution for $\mathbf{u}$ in Stokes equations in terms of $\mathbf{f}$.
The Fourier series coefficient $\mathcal{F}(f)_\mathbf{k}$ with wavevector $\mathbf{k}$ of a function f on the volume $V = [0, L)^3$ is taken to be

$$\mathcal{F}(f)_\mathbf{k} = \int_V f(\mathbf{x}) e^{-\frac{2\pi}{L} i(\mathbf{k}\cdot\mathbf{x})} d\mathbf{x}. \tag{4}$$

The coefficients for the gradient coefficients are thus

$$\mathcal{F}(\nabla f)_\mathbf{k} = \frac{2\pi}{L} i\mathbf{k}\mathcal{F}(f)_\mathbf{k}. \tag{5}$$

Taking the Fourier transform of (1) and (2) yields a new set of equation.

$$\mathbf{k}\cdot\mathcal{F}(\mathbf{u})_\mathbf{k} = 0 \tag{6}$$

$$-\mu\left(\frac{2\pi}{L}\right)^2 |\mathbf{k}|^2\mathcal{F}(\mathbf{u})_\mathbf{k} = i\frac{2\pi}{L}\mathbf{k}\mathcal{F}(p)_\mathbf{k} - \mathcal{F}(\mathbf{f})_\mathbf{k} \tag{7}$$

By taking the dot product of (7) and using (6) to eliminate $\mathcal{F}(\mathbf{u})_\mathbf{k}$, a solution for $\mathcal{F}(p)_\mathbf{k}$ is found. Substituting $\mathcal{F}(p)_\mathbf{k}$ in (7) yields a solution for $\mathcal{F}(\mathbf{u})_\mathbf{k}$, $\mathbf{k} \neq \mathbf{0}$, in terms of $\mathcal{F}(\mathbf{f})_\mathbf{k}$. Finding $\mathbf{u}$ is then a matter of applying the inverse Fourier transform.

$$\begin{aligned}
\mathcal{F}(p)_\mathbf{k} &= -i\frac{\mathbf{k}\cdot\mathcal{F}(\mathbf{f})_\mathbf{k}}{|\mathbf{k}|^2 2\pi/L} \\
\mathcal{F}(\mathbf{u})_\mathbf{k} &= \frac{1}{\mu|\mathbf{k}|^2}\left(\frac{2\pi}{L}\right)^2\left(\mathcal{F}(\mathbf{f})_\mathbf{k} - \mathbf{k}\frac{\mathbf{k}\cdot\mathcal{F}(\mathbf{f})_\mathbf{k}}{|\mathbf{k}|^2}\right)
\end{aligned} \tag{8}$$

However, $\mathcal{F}(\mathbf{u})_\mathbf{0}$ is not defined here. This Fourier coefficient corresponds to the mean velocity of the fluid. It is undefined since the Stokes equations in (1) and (2) only relate to the derivatives of $\mathbf{u}$. A common assignment of this value is $\mathcal{F}(\mathbf{u})_\mathbf{0} := 0$. This is expressed in real space as

$$\int_V \mathbf{u}(\mathbf{x})d\mathbf{x} = 0. \tag{9}$$

In physical terms: there is no net flow over the boundaries of the box.

2.3 Discretization

The velocity field $\mathbf{u}$ in $[0, L)^3$ is represented by a set of values $\mathbf{u_m} := \mathbf{u}(h(\mathbf{m} - \mathbf{1}))$, for $\mathbf{m} \in I = \{(i, j, k)|i, j, k = 1, 2, ..., N\}$, $h = L/N$ and $\mathbf{1} = (1, 1, 1)$. In other words the field $\mathbf{u}$ is described on a cubic $N \times N \times N$-grid by $\mathbf{u_m}$, $\mathbf{m} \in I$. The forcing function is analogously represented by the values $\mathbf{f_m}, \mathbf{m} \in I$. The Stokes flow is calculated directly from $\mathbf{f_m}$ in (8) using the fast Fourier transform (FFT) in Matlab. The 3D discrete Fourier transform $\hat{f}_\mathbf{k}, \mathbf{k} \in I$ of a function representation $\mathbf{f_m}, \mathbf{m} \in I$ is given by

$$\hat{f}_\mathbf{k} = \sum_{\mathbf{m}\in I} f_\mathbf{m} e^{-i\frac{2\pi}{N}\mathbf{k}\cdot(\mathbf{m}-\mathbf{1})}.$$

The continuous Fourier transform (4) can be approximated using the discrete Fourier transform,

$$\mathcal{F}(f) = \int_V f(\mathbf{x})e^{-\frac{2\pi}{L}i(\mathbf{k}\cdot\mathbf{x})}d\mathbf{x} \approx h^3 \sum_{\mathbf{m}\in I} f_\mathbf{m} e^{-i\frac{2\pi}{L}\mathbf{k}\cdot h(\mathbf{m}-\mathbf{1})} = h^3 \cdot \hat{f}_\mathbf{k}. \tag{10}$$

Given $\mathbf{f_m}$ the discretized velocity field $\mathbf{u_m}$ can be calculated from (8) with the FFT, yielding a solution to the discretized Stokes equations.
The FFT can be seen in (10) to approximate the Fourier transform by the trapezoidal rule for periodic functions, using the periodicity to eliminate one boundary term. This circumvents the comparatively low accuracy of the trapezoidal rule.
This gives the FFT spectral convergence in N, given that the function being discretized is C^∞. The accuracy of the solutions for $\mathbf{u}$ in (8) is therefore depending on the smoothness of the input, the forcing function $\mathbf{f}$.

2.4 Regularization

The only contribution to the forcing function in this study is the force of gravity on the system of M particles,

$$\mathbf{f}(\mathbf{x}) = -\rho g\hat{\mathbf{z}} \sum_{i=1}^{M} \delta(\mathbf{x} - \mathbf{x}_i) \approx -\rho g\hat{\mathbf{z}} \sum_{i=1}^{M} \delta^r(\mathbf{x} - \mathbf{x}_i) \tag{11}$$

where ρ is the relative density of the fluid and the particles, g is the gravitational constant and $\hat{\mathbf{z}} = (0, 0, 1)$. $\mathbf{x}_i$ is the position of particle i, $i = 1, 2, ..., M$. To evaluate the singular function in (11) on the grid an interpolating function δ^r is introduced in place of δ. This process is called *regularization*. This is neccessary as directly evaluating a Dirac delta function on a discrete grid will almost always be identical to 0. By introducing a well-chosen wider, continuous "delta-like" function the function behaves nicely on the grid as well, as can be seen in figure 1.

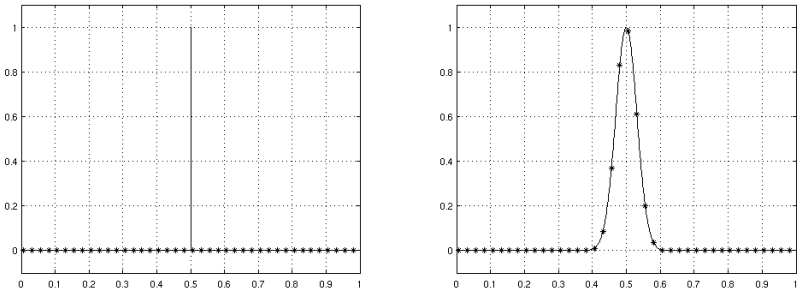

Figure 1: Shows the result of evaluating a Dirac delta function and a delta-like function (lines) on a grid (asterisks). Except for in special cases, the result will come out as 0 for the Dirac deltas while the continuous function will yield better results.

Three conditions are imposed on this *regularization funtion*:

1. $\sum_{\mathbf{m}\in\mathbb{Z}^3} h^3\delta^r(h\mathbf{m} - \mathbf{x}_0) = 1$ for all $\mathbf{x}_0$. This is a discrete version of $\int \delta(\mathbf{x})d\mathbf{x} = 1$.
2. δ^r should be as smooth as possible. The smoothness determines the convergence of solutions to (8).
3. δ^r should have a small, compact support. This allows for relatively cheap calculation of the forcing function in real space.

Two such choices of functions are discussed in this report, mainly based on the methods in [3] and [6]. These choices for δ^r are constructed from univariate functions, $\delta^r(\mathbf{x}) = \delta_1^r(x)\delta_1^r(y)\delta_1^r(z)$.

2.4.1 Triangle functions

Perhaps the simplest choice of δ_1^r is

$$\delta_1^r(x) = \frac{1}{\epsilon} max\left(1 - \frac{|x|}{\epsilon}, 0\right), \tag{12}$$

for some small ϵ. This function is displayed in 2. For $\epsilon = ph$, $p \in \mathbb{Z}^+$, this choice of δ^r does indeed satisfy the first condition.

$$\sum_{\mathbf{m}\in\mathbb{Z}^3} h^3\delta^r(h\mathbf{m} - \mathbf{x}_0) = \sum_{i\in\mathbb{Z}}\sum_{j\in\mathbb{Z}}\sum_{k\in\mathbb{Z}} h\delta_1^r(hi - x_0)h\delta_1^r(hj - y_0)h\delta_1^r(hk - z_0) \tag{13}$$

which by translation symmetry is equal to the cube of

$$\begin{aligned}
\sum_{i\in\mathbb{Z}} h\delta_1^r(hi - x_0) &= \sum_{i\in\mathbb{Z}} h \cdot \frac{1}{\epsilon} max\left(1 - \frac{|hi - x_0|}{\epsilon}, 0\right) \\
&\{wlog\ x_0 \in [0, h)\} \\
&= \frac{h}{\epsilon} \sum_{i=-(p-1)}^{p} 1 - \frac{|hi - x_0|}{\epsilon} \\
&= \frac{2hp}{\epsilon} - \sum_{i=1}^{p} \frac{hi - x_0}{\epsilon^2} - \sum_{i=-(p-1)}^{0} \frac{x_0 - hi}{\epsilon^2} \\
&= \frac{2hp}{\epsilon} - \frac{2h}{\epsilon^2}\left(2\frac{p(p+1)}{2} - p\right) \\
&\{hp = \epsilon\} \\
&= 1
\end{aligned}$$

The function is continuous but without a continuous derivative. Therefore the Fourier coefficients of δ^r decrease as k^{-1}.

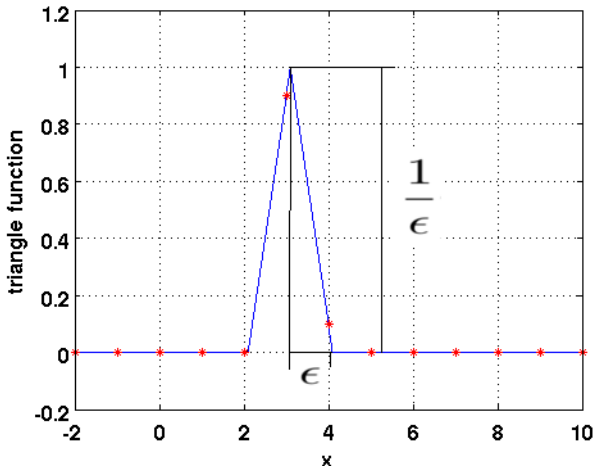

Figure 2: Qualitative image of the triangle function choice of δ^r.

2.4.2 Cardinal splines

Another choice of δ_1^r is found by using the cardinal B-splines M_p of integer order p, $p \geq 2$ described in [1] and [3] and displayed in figure 3,

$$M_p(u) = \frac{1}{(p-1)!} \sum_{j=0}^{p} (-1)^j \frac{p!}{j!(p-j)!} (u-j)_+^{p-1} \tag{14}$$

where $(x)_+ := max(x, 0)$. M_p is nonzero on $(0, p)$ and is shown in [1] to satisfy the following recursive relations with $M_2(u) = (1 - |u-1|)_+$,

$$M_p(u) = \frac{u}{p-1} M_{p-1}(u) + \frac{p-u}{p-1} M_{p-1}(u-1) \tag{15}$$

$$\frac{d}{du} M_p(u) = M_{p-1}(u) - M_{p-1}(u-1) \tag{16}$$

The regularization function is

$$\delta_1^r(hi - x_0) = h^{-1} \cdot M_p(h^{-1}(hi - x_0) + \frac{p}{2})$$

where the term $\frac{p}{2}$ translates the function graph to be symmetric around $hi = x_0$. This function is nonzero for $|hi - x_0| \leq \frac{ph}{2} \Leftrightarrow i \in (\frac{x_0}{h} - \frac{p}{2}, \frac{x_0}{h} + \frac{p}{2})$. The resulting δ^r satisfies the first condition. It splits into a cube as in (13), and

$$\begin{aligned} \sum_{i \in \mathbb{Z}} h\delta_1^r(hi - x_0) &= \sum_{i \in \mathbb{Z}} h \cdot h^{-1} \cdot M_p(h^{-1}(hi - x_0) + \frac{p}{2}) \\ &= \sum_{i=0}^{p} M_p(i + \xi) \end{aligned} \tag{17}$$

for some $\xi \in [0, 1)$ because of translation symmetry and the compact support $[0, p]$ of M_p. $\sum_{i=\xi}^{p+\xi}$ is taken to mean that i is taken in increments of 1. By using the recursion in (15) the expression in (17) can be shown to be 1 by induction. M_2 is in fact a triangle function from section 2.4.1 and has already been proven to sum to 1· Assuming (17) equals 1 for $p-1$ and any ξ,

$$\begin{aligned} \sum_{i=\xi}^{p+\xi} M_p(i) &= \frac{1}{p-1} \sum_{i=\xi}^{p+\xi} iM_{p-1}(i) + (p-i)M_{p-1}(i-1) \\ &= \sum_{i_1=\xi}^{p+\xi} M_{p-1}(i_1 - 1) + \frac{1}{p-1} \sum_{i_2=\xi}^{p+\xi} i_2 M_{p-1}(i_2) - \frac{1}{p-1} \sum_{i_3=\xi}^{p+\xi} (i_3 - 1) M_{p-1}(i_3 - 1) \\ &= \{j_1 = i_1 - 1,\, j_2 = i_2,\, j_3 = i_3 - 1\} \\ &= \sum_{j_1=\xi}^{(p-1)+\xi} M_{p-1}(j_1) + \frac{1}{p-1} \sum_{j_2=\xi}^{p+\xi} j_2 M_{p-1}(j_2) - \frac{1}{p-1} \sum_{j_3=\xi}^{p+\xi} j_3 M_{p-1}(j_3) \\ &= 1. \end{aligned}$$

With the substitution, some first and last terms of the sums are 0 and are removed. The final equality comes from the induction assumption for the first sum. The second and third sum are identical except for the sign, so they cancel, which proves the first condution.
As M_2 is continuous it is easily deduced from (16) that M_p is continuously differentiable $p-2$ times.

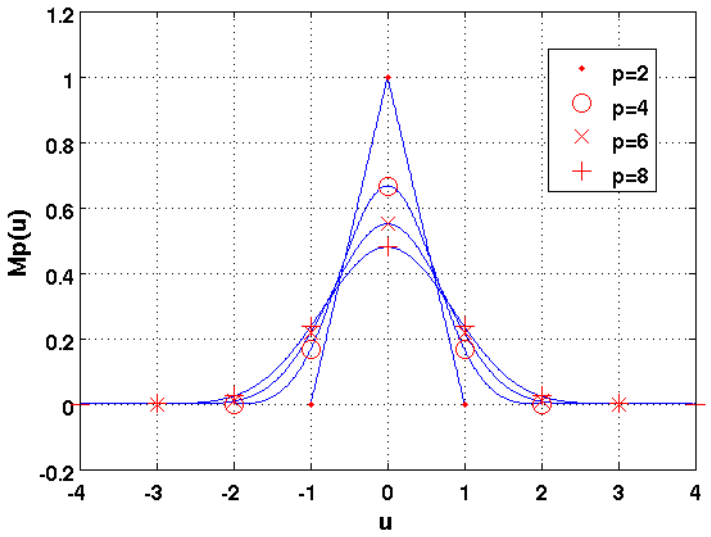

Figure 3: Comparison of the first four even orders of cardinal B-splines, translated to be symmetric in the origin.

2.5 Another method of calculation

The particle velocities can be found directly without gridding by analytically solving the Stokes eqautions for the Dirac delta forcing functions in (11). This method is explored in more detail in [4]. The resulting velocity of particle i is

$$\dot{\mathbf{x}} = \mathbf{U}_0 + \rho g \hat{\mathbf{z}} \cdot \sum_{i \neq j} \mathbf{T}(\mathbf{x}_i - \mathbf{x}_j). \tag{18}$$

where $\mathbf{U}_0$ is the mean velocity of the fluid and the terminal settling velocity of an isolated particle. As in (9) it is common to eliminate this term by choosing the frame of reference moving with the velocity $\mathbf{U}_0$. $\mathbf{T}(\mathbf{r})$ is the Oseen-Burgers tensor,

$$\mathbf{T}(\mathbf{r})_{ij} = \frac{1}{8\pi\mu|\mathbf{r}|}\left(\delta_{ij} + \frac{\mathbf{r}_i\mathbf{r}_j}{|\mathbf{r}|^2}\right)$$

in Einstein notation.
The complexity issues with this approach relates to the number of particles M. The computational cost of calculating the sum in (18) is $O(M^2)$.

3 Setup and algorithms

3.1 The scene

The system in question is a cloud of M particles randomly placed within a sphere of radius r_0. This sphere begins in the center of a primitive cell, a cube of side length L, which is periodically repeated throughout space.
The particles are affected by a gravitational force downward and a lift from the fluid. The resulting force on the particles is the sole driving force in the simulation.
The force from the particles on the fluid make up the forcing function in Stokes' equation.

3.2 The four-step simulation

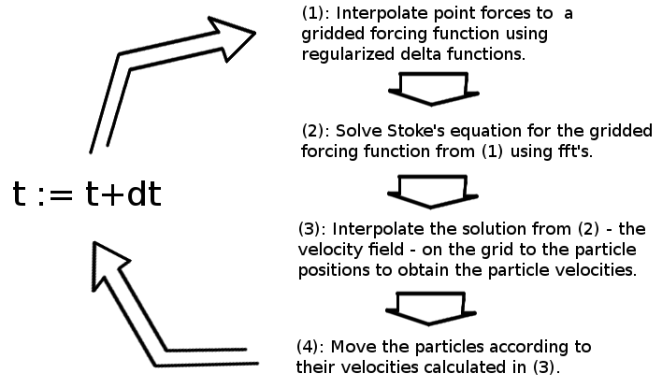

Figure 4: The simulation algorithm steps

Each timestep the simulation has four distinct moments, as illustrated in figure 4.

1. Interpolating from particle positions to grid positions
   The gravitational force on the particles manifests as singular functions in the Stokes' equation forcing function. To evaluate this force on the grid, the singular functions are regularized to the grid by representing them with regularized δ-functions and evaluating these on the grid.
   This interpolates the M point forces to a forcing function on the N^3-grid.

2. Solving Stokes' equation
   Given the forcing function it is a matter of solving Stokes' equation. This is done using the fft (and thereby the periodicity assumption), giving the following formula derived in appendix.

3. Interpolate the velocity field to the particle positions
   This is simply done by cubic interpolation using Matlab's builtin function *griddata*.

4. Timestepping the particles
   Given the particle velocities, the particles' positions can now be calculated using Euler's method.

If the only interest is studying the velocity field solution on the grid, steps 1-2 are sufficient. This can be done for any time t in the simulation, as Stokes' equation is *memoryless*, it does not depend on the history of neither the velocity field nor the forcing functions.

3.3 The particle cloud setup used here

Two systems of particles are studied in this article. One The first and simplest systems has $M = 3$ particles placed along a central z-axis in the primitive cell, two clustered to display the increase in velocity as they drag more fluid together. The second, larger system has a cloud of M 10^3 particles uniformly distributed over a ball, initially in the center of the primitive cell. This is similar to the system studied in [4].

4 Results

4.1 Properties of the simulation method with few particles

4.1.1 Convergence of the Stokes flow

The convergence of the solution obtained through (8) depends on the smoothness of the forcing function $\mathbf{f}$. The convergence of solutions for a smooth and a non-smooth forcing function can be seen in figure 5, solved in a cube with $L = 2.0$. The smooth function is g_1 and the non-smooth, once continuously differentiable function is g_2.

$$g_1(x,y,z) = \sin(L\cos(\frac{2\pi}{L}x))\cos(\frac{2\pi}{L}y) + \sin(\frac{2\pi}{L}z),$$
$$g_2(x,y,z) = \sin(\frac{2\pi}{L}x)\cos(\frac{2\pi}{L}y)(\frac{2}{L^2}z^3 - \frac{3}{L}z^2 + z).$$

The non-smooth solution converges as $N^{-2.06}$ while the smooth solution is clearly exponential.

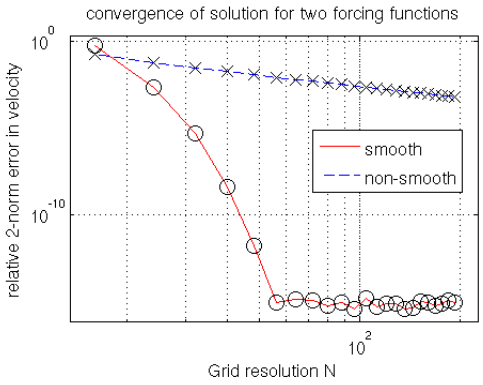

Figure 5: Convergence of the Stokes flow solutions for a smooth and a non-smooth forcing function.

4.1.2 Characteristics of solutions for regularized singular forcing functions

Here the forcing function in equation (11) is introduced. A simple system consisting of a periodic cube of side length $L = 2.0\ m$. $M = 3$ particles are placed along the central z-axis at heights 0.9, 1.1 and 1.2 m. $N = 256$.
Using different regularization functions in the forcing function yields different solutions for $\mathbf{u}$. The particle positions and forcing functions along the central z-axis are plotted for different choices of regularization function in figures 6 and 8. The solved Stokes flow along the same axis are plotted in figures 7 and 9.
Note that while the delta functions appear to have different area, they still sum to 1. A function with narrower support is not as spread out in the x- and y-direction and appears larger in the plots.

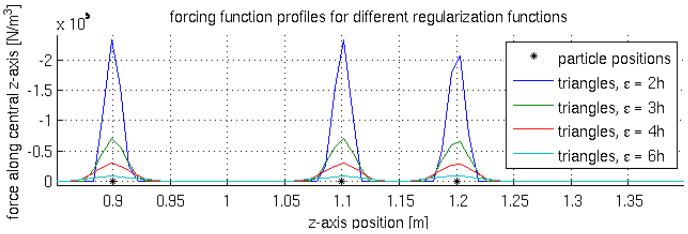

Figure 6: The forcing function evaluated on the central z-axis for different widths of triangle functions.

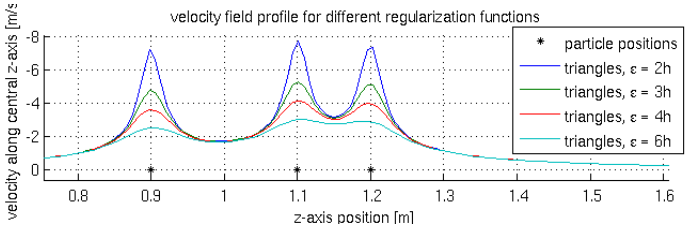

Figure 7: The u_3-component of $\mathbf{u}$ along the central z-axis for different widths of triangle functions.

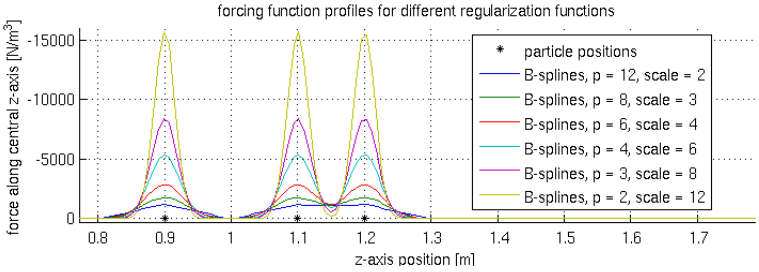

Figure 8: The forcing function evaluated on the central z-axis for different orders of Cardinal B-Spline forcing functions, keeping the support fixed.

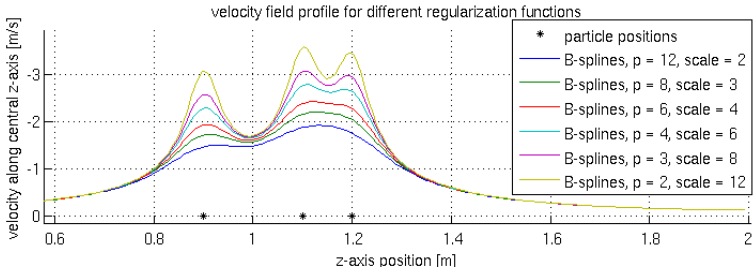

Figure 9: The u_3-component of $\mathbf{u}$ along the central z-axis for different orders of Cardinal B-Spline forcing functions, keeping the support fixed.

In the velocity plots, figures 7 and 9, the forcing functions with narrower support appear more like delta functions, explaining that the Stokes flow has sharper and higher velocity peaks near the particle position.
The narrow regularization functions resemble the non-regularized Stokes flow solution, with singularities in particle positions. The wider functions yield a more spread out solution, implying these "smeared" particles affect fluid and particles further away. However,

the Stokes flows are indistinguishable in the plots only a short distance from the 3-particle cluster.
This is observed regardless of whether it is the scale that is increaed - figure 7 - or the spline order while keeping the support fixed - figure 9. This implies that if a triangular regularized delta function with wide support is used, a similar solution behaviour might be obtained with a higher order B-spline and smaller support.

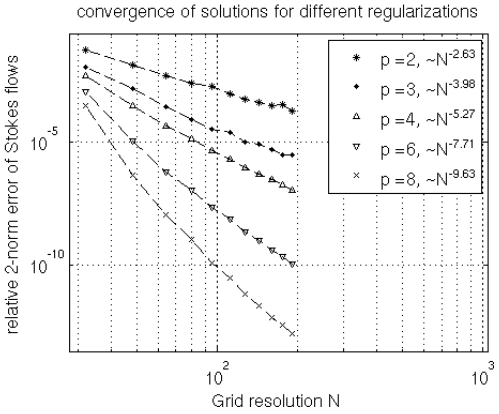

Figure 10: Convergence of the Stokes flow solutions for the three particles with different choices of regularization, where $N = 16n$, $n = 1, 2, ..., 11$.

Figure 10 shows the convergence of different orders of B-splines. Each relative error is calculated from two Stokes flow solutions $\mathbf{u}^{nN_0}$ and $\mathbf{u}^{(n+1)N_0}$ for given integers $N_0 = 16$ and $n = 1, 2, ..., 11$ and a fixed spline order.

$$y(nN_0) = \frac{\|\mathbf{v}^{(n+1)N_0} - \mathbf{v}^{nN_0}\|_2}{\|\mathbf{v}^{nN_0}\|_2}, \tag{19}$$

where $\mathbf{v}^{nN_0}$ contains the elements $\mathbf{u}_{kn}^{nN_0}$, $k = 1, 2, ..., N_0$ to compare vectors of different length. N is taken to be nN_0.
The solutions clearly converge as N increases. Higher order splines yields faster convergence. If higher accuracy is required, increasing the spline order could be a good way of achieving it if the application allows for the wider support that comes with higher spline order.

4.1.3 Convergence of the triangular forcing functions as N increases

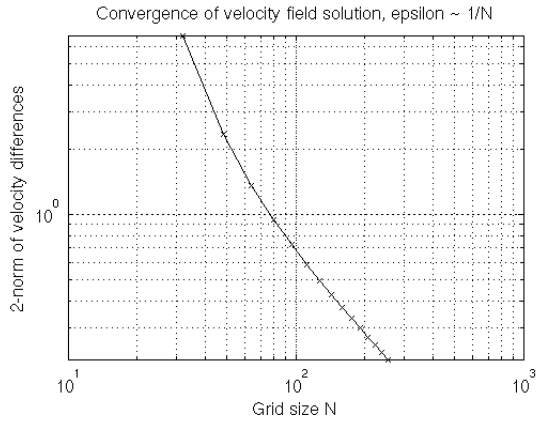

Figure 11: Normed successive differences in solutions as N increases and epsilon decreasing with it.

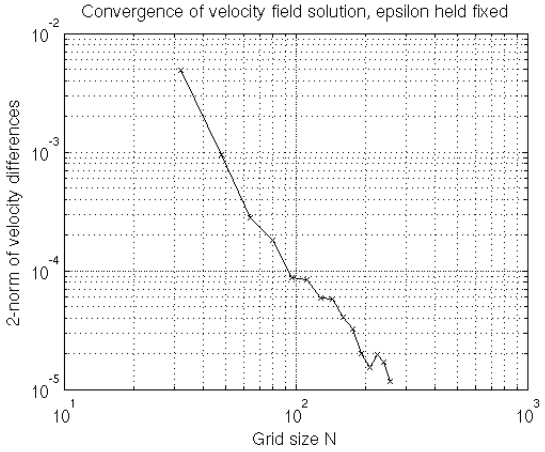

Figure 12: Normed successive differences in solutions as N increases, keeping epsilon fixed.

4.1.4 Scaling the primitive periodic cell

If the cloud of particles is of the same magnitude as the period L of the system it is not unlikely to have interactions between clouds of different primitive cells. The effect of this is be studied by scaling the length of the primitive cells while keeping the particle cloud size fixed and looking at the differences between successive solutions for the velocity field in a cube of fixed size containing the particle cloud. The result is displayed in figure

13. For simple triangle functions, the successive relative differences decrease as $L^{-1.30}$. While the meaning of this measure in not entirely obvious, since for each value of L a different physical system is studied, the solutions for these systems should converge to the non-periodic case as $L \to \infty$.

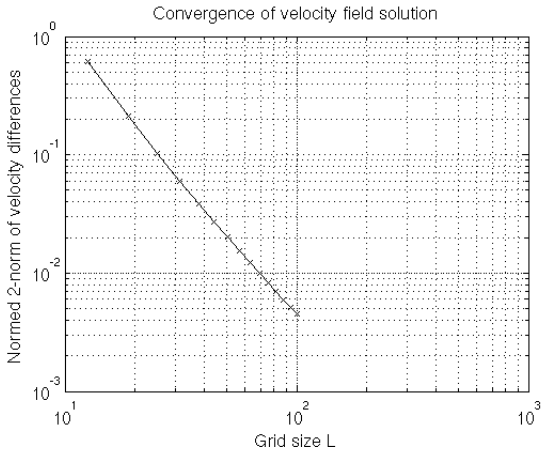

Figure 13: Normed successive differences in solutions as the primitive cell increases.

4.2 Macroscopic phenomena

The evolution of the cloud shape in a periodic box appears to agree to some extent with that observed by Metzger et al [4] in a non-periodic setting. A simulation was run with $M = 1000$ particles randomly uniformly scattered inside a ball of radius 0.5 where $L = 2\pi$ and simulated with a mesh size of $N = 64$ and $dt = 0.01$. The sedimenting particle cloud becomes oblate, forms a torus and eventually breaks into two smaller clouds, as can be seen in Figure 14 and 15.

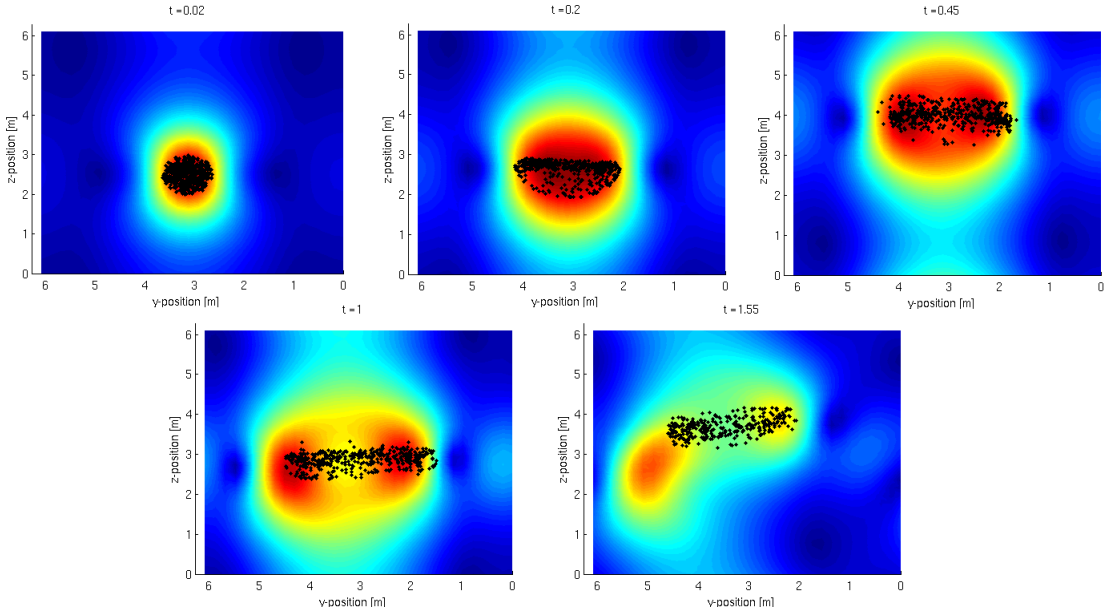

Figure 14: Some frames characterizing the stages the particle cloud undergoes as it sediments. The color indicates qualitatively the fluid speed in a cross section at $x = 0.5L$. The time frames are read from left to right, top row first.

Figure 15: A different angle of the simulation in figure 14 from a different angle and slightly later time. Note the split into two different particle clouds, as well as the trailing tail of particles leaving the cloud.

For too few gridpoints the cloud appears to take a square shape aligned with the grid cells, see Figure 16. When this effect in practice disappears can be studied further, e.g. by plotting the particle density as a function of azimuthal angle.

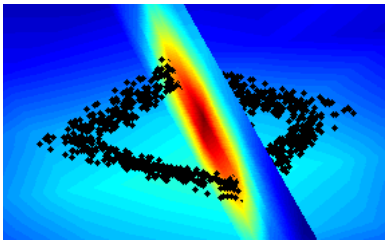

Figure 16: The square shape of the torus cloud for N=8 [plot missing axes, units, #steps, dt=0.001, N=8, M=1000 etc]

5 Conclusions

The choice of regularization function directly influences the solutions for the Stokes equations. Wider choices of δ^r do not mirror the behaviour of the analytical, non-regularized solution, at least not locally. They might be more suitable for simulating particles with a less defined radius. On the other hand, to choose narrower functions means either less accurate solutions or a finer calculation grid.
By comparing this method to exact solutions for spherical particles one could try to find at what support size - what *efficient radius* - would behave most like the spherical particle solutions.
The convergence in N of Stokes flow solutions for different splines was not investigated enough for inclusion in this thesis, and would be a logical next step after the triangle functions in examining these different δ^r.
To eliminate all unwanted properties of the periodicity and regularization in the larger simulation requires a large N, which might push the computations into a less feasibly computed range.
However, the grid only needs to be finer by the particle - in and near the support of the regularized delta functions. One way of handling this could be by using some non-uniform gridding method and the non-uniform FFT.
For larger systems this method seems to capture at least some properties of the behaviour non-periodic non-regularized system, unless N is taken to be too small. By running comparisons with similar methods, e.g. by looking at statistical measures of the particle cloud, one could explain more of the behaviour of this system and what makes it behave differently the way it does.
There are three ways in which this system deviates from the original physical system of particles in free space. It has been discretized, periodic and point particles have been replaced by regularized delta functions. All of these steps takes us further away from the physical system and introduces new proprties of the system, and careful studies are needed.

References

[1] Ulrich Essmann, Lalith Perera, Max L. Berkowitz, Tom Darden, Hsing Lee, and Lee G. Pedersen. A smooth particle mesh ewald method. *The Journal of Chemical Physics*, 103:8577–8593, 1995.

[2] Élizabeth Guazzelli and Jeffrey F. Morris. *A Pysical Introduction to Suspension Dynamics*. Cambridge University Press, 1 edition, 2012.

[3] Dag Lindbo and Anna-Karin Tornberg. Spectral accuracy in fast ewald-based methods for particle simulations. *Journal of Computational Physics*, 230:8744–8761, 2011.

[4] Bloen Metzger, Maxime Nicolas, and Élizabeth Guazzelli. Falling clouds of particles in viscous fluids. *J. Fluid Mech.*, 580:283–301, 2007.

[5] David Saintillan, Eric S.G. Shaqfeh, and Eric Darve. The growth of concentration fluctuations in dilute dispersions of orientable and deformable particles under sedimentation. *J. Fluid Mech.*, 553:347–388, 2006.

[6] Anna-Karin Tornberg and Björn Engquist. Numerical approximations of singular source terms in differential equations. *Journal of Computational Physics*, 200:462–488, 2004.